SU(N) magnetism with ultracold molecules

Bijit Mukherjee,[1] Jeremy M. Hutson,[1,*] and Kaden R. A. Hazzard[2,3,†]

[1] *Joint Quantum Centre (JQC) Durham-Newcastle, Department of Chemistry, Durham University, South Road, Durham, DH1 3LE, United Kingdom.*
[2] *Department of Physics and Astronomy, Rice University, Houston, Texas 77005, USA*
[3] *Smalley-Curl Institute, Rice University, Houston, Texas 77005, USA*

(Dated: April 25, 2024)

Quantum systems with SU(N) symmetry are paradigmatic settings for quantum many-body physics. They have been studied for the insights they provide into complex materials and their ability to stabilize exotic ground states. Ultracold alkaline-earth atoms were predicted to exhibit SU(N) symmetry for $N = 2I+1 = 1, 2, \ldots, 10$, where I is the nuclear spin. Subsequent experiments have revealed rich many-body physics. However, alkaline-earth atoms realize this symmetry only for fermions with repulsive interactions. In this paper, we predict that ultracold molecules shielded from destructive collisions with static electric fields or microwaves exhibit SU(N) symmetry, which holds because deviations of the s-wave scattering length from the spin-free values are only about 3% for CaF with static-field shielding and are estimated to be even smaller for bialkali molecules. They open the door to N as large as 32 for bosons and 36 for fermions. They offer important features unachievable with atoms, including bosonic systems and attractive interactions.

I. INTRODUCTION

The prediction and experimental realization of SU($N = 2I + 1$) symmetry in ultracold alkaline-earth atoms [1–4] with nuclear spin I has allowed the study of a wealth of phenomena: bosonization of high-spin fermions by measurements of collective modes [5–7], flavor-selective Mott transitions in a lattice [8], and the SU(N) Fermi-Hubbard model's equations of state [9–11] and short-ranged magnetic correlations [12]. The symmetry is also responsible for the temperature $T = 1\,\mathrm{nK}$ reached in Ref. [12]; this is the lowest temperature ever achieved for fermions. Unlike ordinary SU(2) spins, quantum fluctuations need not become classical for large spin. Consequently, exotic behavior is predicted to occur in lattices as the temperature is lowered further. Predicted phases abound for different lattice geometries and N, including chiral spin liquids, a topological phase of matter never before observed [13, 14]. The itinerant or doped SU(N) Hubbard models are little explored and likely to show extremely rich phenomena.

However, alkaline-earth-atom realizations of SU(N) physics have important limitations. One constraint is that, to have $I \neq 0$ ($N > 1$), such atoms must be fermions to satisfy the "even-even" rule of nuclear physics [15]. Another constraint is that, empirically, all the interactions in the experimentally viable ultracold alkaline-earth atoms, Sr and Yb, are repulsive, i.e., have a positive scattering length a [4]. Moreover, the important tool of magnetic Feshbach resonances that is used to tune interactions in alkali atoms is absent for ground-state alkaline-earth atoms, since they lack unpaired electrons.

Rapidly advancing experiments with ultracold molecules offer exciting possibilities for many-body physics, quantum technologies, precision measurement, and studying chemical reactions [16–20]. A wide variety of ultracold molecules have been produced [16], including alkali-metal dimers produced by assembly of ultracold atoms, and other species produced by direct laser cooling. Experiments revealed losses that occur when molecular collisions reach short range ($R \lesssim 100\ a_0$), which impede the creation of interesting many-body states. They occur for both reactive and non-reactive molecules. This discovery stimulated theoretical proposals to shield the molecules from short-range loss by creating intermediate-range repulsive interactions using static electric fields [21–25] or microwave radiation [26, 27]. These have now been demonstrated experimentally [28–34]. Notably, Bose-Einstein condensation has recently been achieved for NaCs using two-color microwave shielding [35].

In this paper, we show that shielded molecules can realize SU(N) systems that circumvent the constraints of alkaline-earth atoms, and introduce other interesting properties. Fermionic and bosonic molecules are available, and the sign and magnitude of the scattering length can be tuned by varying the control fields that generate the shielding [25, 27]. The dipolar interactions may also be tuned. Experimentally available molecules can realize all N up to $N = 36$, for $Na^{40}K$ [32], much larger than for Sr ($N = 10$) and Yb ($N = 6$).

The properties of SU(N) molecular systems open interesting paths for many-body physics. Attractively interacting SU(N) systems are predicted to have rich pairing structures, for example transitions between color superfluid and trion phases [36–41], with similarities to the crossover from a confining hadronic phase to a parton gas in high-energy physics [42]. Bosonic SU(N) systems have garnered interest as integrable systems [43], holographic duals [44], and ferromagnets with non-Abelian symmetry breaking [45]. Such examples offer a small glimpse of the possibilities offered by shielded ultracold molecules.

* j.m.hutson@durham.ac.uk
† kaden.hazzard@gmail.com

Section II presents coupled-channel calculations for CaF collisions shielded with a static electric field. Even CaF, which has much larger spin couplings than bialkali molecules, satisfies SU(N) symmetry to about 3% relative accuracy. We develop a model to estimate quantitatively the nuclear-spin dependence of interactions for other molecules. This shows that SU(N) symmetry will hold to even higher accuracy for alkali dimers. Section III derives many-body models for these systems, especially the SU(N) Hubbard models that describe shielded molecules in an optical lattice. Section IV summarizes, suggests experiments to verify the predictions, and outlines next steps for the field.

II. SHIELDED INTERACTIONS OF MOLECULES

A pair of polar molecules, $k = 1, 2$, interact at long range via the dipole-dipole interaction

$$\hat{H}_{\rm dd} = -\frac{3(\boldsymbol{\mu}_1 \cdot \hat{\boldsymbol{R}})(\boldsymbol{\mu}_2 \cdot \hat{\boldsymbol{R}}) - \boldsymbol{\mu}_1 \cdot \boldsymbol{\mu}_2}{4\pi\epsilon_0 R^3}, \qquad (1)$$

where R is the intermolecular distance, $\hat{\boldsymbol{R}}$ is the corresponding unit vector, and $\boldsymbol{\mu}_k$ is the dipole moment of molecule k which lies along the molecular axis. For an s-wave collision, with relative angular momentum (partial-wave) quantum number $L = 0$, the dipole-dipole interaction averages to zero. However, it has matrix elements between $L = 0$ and 2, both diagonal and off-diagonal in molecular pair state. The matrix elements off-diagonal only in L cause an effective long-range attraction proportional to d^4/R^4 [46], where d is the space-fixed dipole moment of each molecule (for static-field shielding) or the rotating dipole (for microwave shielding).

Both static-field and microwave shielding operate by engineering a field-dressed pair state to be a small energy ΔE below the initial state of interest. Matrix elements of $\hat{H}_{\rm dd}$ that connect the two pair states produce a repulsive contribution to the interaction potential for the upper (initial) state. Shielding occurs when the repulsion is sufficient to prevent pairs of colliding molecules coming close together. The repulsion is proportional to $(d^4/\Delta E)/R^6$ at long range.

The combination of long-range attraction and shorter-range repulsion produces a potential well at long range, whose depth and position depend on the molecule and the field applied. This allows considerable control over the scattering length, which for some molecules may be tuned from positive to negative values and even through poles [25, 27].

We focus here on static-field shielding, using coupled-channel scattering calculations on CaF as an example. The methods used are described in Ref. [24] and their numerical convergence is described in Methods. We begin with spin-free calculations (Sec. II A) and then consider the effects of electron and nuclear spins (Sec. II B).

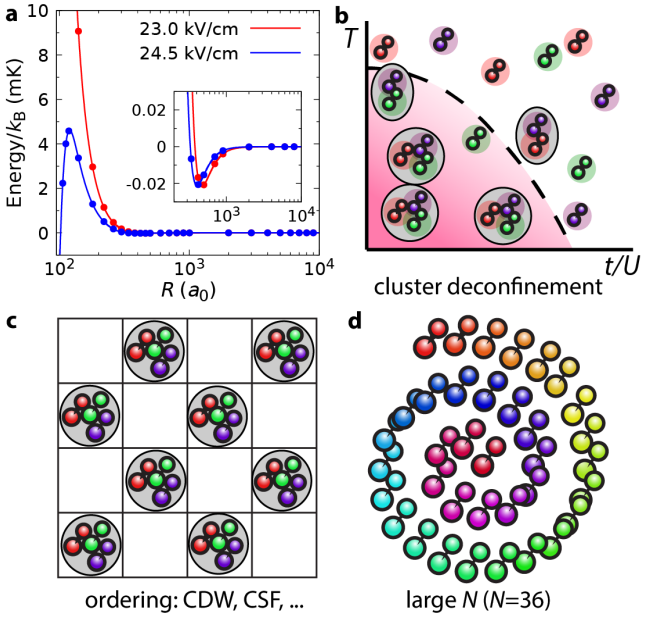

FIG. 1. **SU(N) symmetry in intermolecular interactions and its consequences.** (a) Effective potentials (adiabats) for CaF in the spin state $(g, m_g) = (1, 0)$ (solid circles) are nearly equal to the spin-free adiabats (solid lines) for fields of 23 and 24.5 kV/cm. Adiabats for other spin states are even closer to the spin-free curves. (b-d) Examples of many-body physics enabled by shielded ultracold molecules: (b) formation of bound molecular clusters and their dissociation by thermal (temperature T) or quantum (e.g. lattice tunneling t) fluctuations, reminiscent of deconfinement in QCD, (c) ordered phases in optical lattices including charge density waves (CDW) and color superfluids (CSF), and (d) states with large quantum fluctuations arising from large N and the high degree of symmetry.

A. The spin-free case

We consider collisions between molecules in the state $(\tilde{n}, m_n) = (1, 0)$, for which static-field shielding is most effective. The single-molecule eigenstates are labeled by hindered-rotor quantum numbers $\tilde{n}$, which correlate at zero field with the free-rotor quantum number n, and m_n, its projection onto z.

It is helpful to consider the effective potentials for scattering. We define these as adiabats that are the R-dependent eigenvalues $U_i(R)$ of the pair Hamiltonian given in Methods. Figure 1 shows the spin-free adiabats for s-wave scattering for two CaF molecules in state $(\tilde{n}, m_n) = (1, 0)$ at two values of an applied electric field F that produce effective shielding.

There are two sources of 2-body loss. First, the repulsion does not extend all the way to $R = 0$. There is a repulsive barrier, and some colliding pairs may tunnel through it to reach short range ($R \lesssim 100\ a_0$), where loss may occur. Secondly, there can be inelastic collisions that produce molecules in lower field-dressed states, particularly in the pair state just below the initial one. The solid lines in Fig. 2(a) show the calculated rate coefficients for

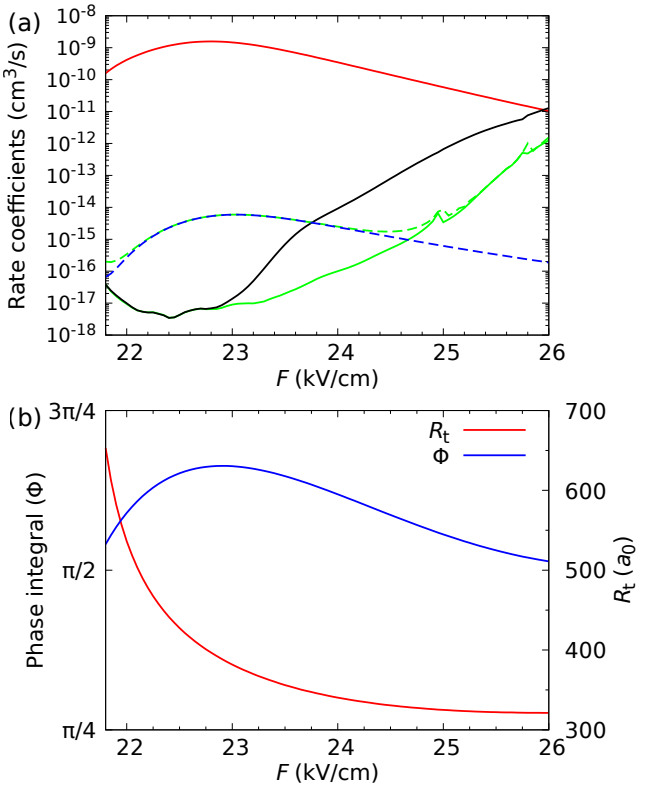

FIG. 2. **Collision rate coefficients and features of the spin-free effective potential for CaF.** (a) Rate coefficients for elastic scattering (red), inelastic scattering (green) and short-range loss (black) for CaF at collision energy $E_{\rm coll} = 10$ nK $\times$ $k_{\rm B}$, over the range of electric fields where shielding is effective. The calculations use the spin-N206-L6 basis set described in Methods. Solid lines show spin-free calculations. Dashed lines show the corresponding results for initial $(g, m_g) = (1, 1) + (1, 1)$. The blue dashed line shows the contribution from the 1-molecule inelastic transition to (1,0). (b) The inner turning point $R_{\rm t}$ (red) and phase integral Φ (blue) over the same range of field.

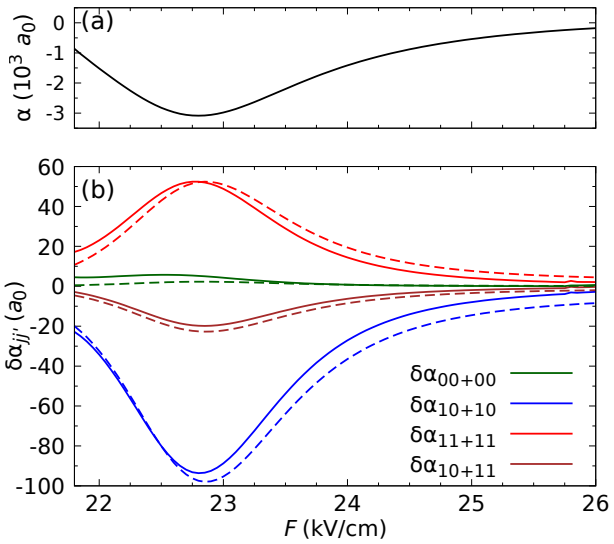

FIG. 3. **Effect of spins on scattering length.** (a) Real part $\alpha(F)$ of the scattering length for CaF from spin-free calculations. (b) Scattering lengths $\alpha_{jj'}(F)$, including the effects of spin, shown as differences from field-free values. Solid lines are from coupled-channel calculations; dashed lines are from the model of Eq. 4. Each spin combination is labeled by $gm_g + g'm'_g$.

spin-free elastic scattering and total (inelastic + short-range) loss for CaF as a function of F [24]. The overall effectiveness of shielding may be characterized by the ratio γ of rate coefficients for elastic scattering and loss; this can be up to 10^7 for CaF and much larger for molecules such as NaCs [25]. The calculations also provide the complex s-wave scattering length, $a(F) = \alpha(F) - i\beta(F)$, where β arises due to loss and L-changing collisions and is small when shielding is effective. The real part $\alpha(F)$ is of principal interest here. Figure 3(a) shows $\alpha(F)$ for CaF from spin-free coupled-channel calculations.

B. Dependence on spin state

SU(N) symmetry exists when the shielded interactions are almost independent of molecular spin state and diagonal in it. Here we describe an approach to estimate the dependence on spin state and present quantum scattering calculations for CaF that validate the estimate. We then give estimates of the spin dependence for a variety of ultracold molecules of current experimental interest.

Electron and nuclear spins are described by the Hamiltonian for fine and hyperfine structure, $\hat{h}_{\rm fhf}$, given in Methods. For CaF in a strong electric field, the electron spin $s = 1/2$ and the nuclear spin $i = 1/2$ of ^{19}F couple to form g, with projection m_g; these are approximately conserved and can take values $(g, m_g) = (0, 0)$, (1,0) and $(1, \pm 1)$.

We first diagonalize the single-molecule Hamiltonian, including $\hat{h}_{\rm fhf}$. We calculate the space-fixed dipole moments $d_j = \langle j|\boldsymbol{\mu}_z|j\rangle$ for $j = (\tilde{n}, m_n, g, m_g)$ with $(\tilde{n}, m_n) = (1, 0)$. It is convenient to define fractional changes $\Delta d_j = (d_j - d_0)/d_0$ from the spin-free value d_0. These depend only weakly on F: for CaF at $F = 23$ kV/cm, the values are -1.9×10^{-5}, 8.3×10^{-4} and -4.4×10^{-4} for the states $(g, m_g) = (0, 0)$, $(1, 0)$ and $(1, \pm 1)$, respectively. The coefficient of the long-range attraction is proportional to d_j^4 and thus differs by at most 0.33% from d_0^4. We may expect that the effective potentials will differ by about this amount.

To test this simple model of the interactions, we perform full coupled-channel calculations including electron and nuclear spins for both molecules. Details are in Methods. The calculations produce scattering lengths $a_{jj'}$ and rate coefficients for elastic scattering and loss, as before, but now for each pair of spin states $j = (g, m_g)$ and $j' = (g', m'_g)$. In zero magnetic field there are 7 distinct pairs, because pairs with $(m_g, m'_g) = (0, \pm 1)$ are equivalent, as are the pairs $(\pm 1, \pm 1)$, though the latter

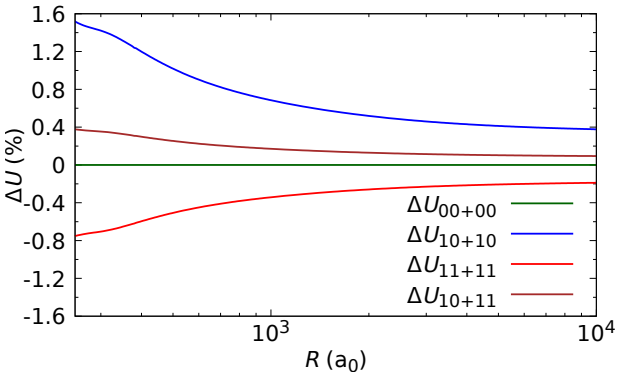

FIG. 4. **Effect of spins on the adiabats.** Fractional differences $\Delta U_{jj'}(R)$ between adiabats with and without spin, defined by Eq. 2, for CaF at 23 kV/cm. Each spin combination is labeled by $gm_g + g'm'_g$.

are different from $(\pm 1, \mp 1)$.

Shielding remains effective for all spin states, even for distinguishable pairs. However, there are additional inelastic transitions for some spin states due to spin-changing collisions. In particular, a molecule initially in $(g, m_g) = (1, 1)$ can undergo a transition to (1,0). The rate coefficient for this process in a collision of two such molecules is shown as a blue dashed line in Fig. 2(a). The elastic and short-range loss are almost unaffected, but the total inelastic loss is modified as shown by the dashed green line. The spin-changing rate coefficients are no larger than 10^{-14} cm^3 s^{-1} and the ratio γ remains above $\sim 10^5$. The spin-changing rates are similar for other collisions involving a molecule in state (1,1), and otherwise very small. This satisfies the requirement that the interactions are diagonal in spin state.

The real part of the scattering length $\alpha(F)$ depends only weakly on spin state. The solid lines in Fig. 3(b) show the differences $\delta\alpha_{jj'}(F) = \alpha_{jj'}(F) - \alpha_0(F)$ between the scattering lengths and the spin-free value $\alpha_0(F)$ of Fig. 3(a) as a function of field. The values $\alpha_{jj'}$ not shown are close to $(\alpha_{jj} + \alpha_{j'j'})/2$. This demonstrates that the scattering lengths are independent of spin state to within about 5% for shielded CaF.

The coupled-channel calculations provide adiabats as in Fig. 1, but now for each spin combination. They are almost indistinguishable on the scale of Fig. 1. However, they cross zero at slightly different inner turning points $R_{tjj'}$, so to show their differences we define

$$\Delta U_{jj'}(R) = \frac{U_{jj'}(R + R_{tjj'} - R_{t0}) - U_0(R)}{U_0(R)}, \quad (2)$$

shifting $U_{jj'}(R)$ slightly in R so that its turning point matches R_{t0}. Fig. 4 shows $\Delta U_{jj'}(R)$ for all spin combinations of CaF at 23 kV/cm. The differences between the adiabats including spin and the spin-free adiabat are no more than 2% over the entire classically allowed range of R. The effective potential for interaction of molecules in spin states j and j' has long-range form

$$U_{jj'}(R) = -\frac{4\hbar^2 D_{jj'}^2}{15\mu_{\rm red} R^4}, \quad (3)$$

where $D_{jj'} = d_j d_{j'} \mu_{\rm red}/(4\pi\epsilon_0\hbar^2)$ is the dipole length for space-fixed dipoles d_j and $d_{j'}$. At large R, the ratios of the adiabats are accurately given by the corresponding ratios of $D_{jj'}^2$.

We have developed a model for the effective potentials and scattering lengths for shielded collisions, which allows simple estimates of the spin-dependence of the scattering length for CaF and other molecules. The model is derived in Methods and gives

$$\frac{d\alpha}{dD} \approx (\alpha - 2R_{\rm t})/D - 2\Phi\sqrt{8/15}\sec^2\left(\Phi - \frac{\pi}{4}\right), \quad (4)$$

where Φ is a phase integral involving the spin-free potential and $R_{\rm t}$ is its zero-energy turning point. These quantities are shown for CaF in Fig. 2(b), as a function of field.

The dashed lines in Fig. 3 show the results of the model for $\delta\alpha_{jj'}$, compared to the coupled-channel results including spin for CaF (solid lines). The model captures the overall behavior well. Details of the model for CaF at 23 kV/cm are given in Extended Data Table I, including the spin combinations not shown in Fig. 3. At this field, Φ for CaF is slightly less than $3\pi/4$; this is close to a pole in α as a function of Φ, with α large and negative. Here the second term in Eq. 4 dominates, and small changes in Φ cause large fractional changes in α. Nevertheless, even for CaF at 23 kV/cm, where d_j varies by up to 0.13% between spin states, the values of $\delta\alpha_{jj'}$ are no more than 3% of α. For systems where Φ is not close to a pole, there will be less amplification of $d\alpha/dD$ by the last term in Eq. 4.

CaF has only 4 spin states, so can be used realize SU(N) up to $N = 4$. Other molecules, particularly alkali dimers, can reach much greater N: singlet molecules with two spin-3/2 nuclei, such as ^{87}Rb^{23}Na or ^{39}K^{23}Na, can reach $N = 16$, while bosonic molecules with larger spins, such as NaCs, can reach $N = 32$. Fermionic ^{40}K^{23}Na can reach $N = 36$.

Alkali dimers have a hyperfine Hamiltonian [47] similar to that for CaF, but with the electron spin replaced by a second nuclear spin and additional terms arising from nuclear quadrupole coupling. Coupled-channel calculations that fully include spin are challenging for these molecules, because the spin space is so much larger: for NaCs, for example, the number of spin functions for the pair is 64 times larger than for CaF, and the computer time scales as the cube of this. Nevertheless, we can estimate the spin dependence, using the understanding gained from CaF. The changes in scattering length from the field-free value are

$$\delta\alpha_{jj'} = (D_{jj'} - D_0)\frac{d\alpha}{dD} \approx D_0\left(\Delta d_j + \Delta d_{j'}\right)\frac{d\alpha}{dD}. \quad (5)$$

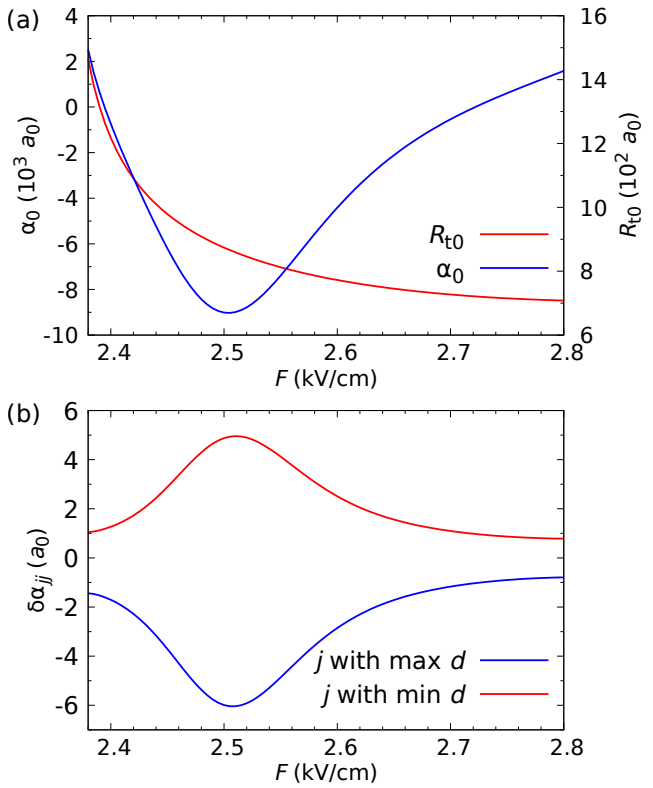

FIG. 5. **Predicting spin-dependent changes in scattering length for NaCs from the model.** (a) Spin-free turning point R_{t0} and real part of scattering length α_0 for NaCs at fields where shielding is effective; (b) Real parts of α_{jj} from Eq. 4, including the effects of spin, shown as differences $\delta\alpha_{jj}$ from field-free values. Results are shown for spin states j with maximum and minimum values of d_j and span the range of possible values of $\delta\alpha_{jj}$.

Molecule	F (kV/cm)	$\lvert(d_{\max} - d_{\min})/d_0\rvert$	R_{t0} (a_0)
RbCs	2.7	4.3×10^{-4}	750
$Na^{39}K$	7.1	8.3×10^{-5}	630
$Na^{40}K$	7.1	8.9×10^{-5}	a
$Na^{41}K$	7.0	1.0×10^{-4}	620
NaRb	4.5	4.9×10^{-4}	650
NaCs	2.5	2.4×10^{-5}	870
CaF	23	1.3×10^{-3}	380

[a]For $Na^{40}K$, which is fermionic, the lowest channel has $L = 1$ and its adiabat never drops below zero energy.

TABLE I. **Spread of dipole moments among different spin states.** Range of dipole moments $(d_{\max} - d_{\min})/d_0$ for different spin states of the field-dressed level $(\tilde{n}, m_n) = (1, 0)$ for alkali dimers and CaF. For each molecule, we choose an electric field where static-field shielding is effective, but the ranges of dipole are only weakly dependent on field. The value of R_{t0} is also given at the chosen field, but this depends much more strongly on field.

Table I summarizes the range of Δd_j across spin states, for several ultracold molecules of current interest, for the field-dressed level $(\tilde{n}, m_n) = (1, 0)$ that can be shielded with a static electric field. All the alkali dimers have ranges substantially smaller than CaF.

NaCs is particularly interesting, because α can be tuned close to zero at $F \approx 2.395$ kV/cm [25], in the region where shielding is effective. It has 32 hyperfine states and a particularly small range of dipoles, because NaCs has unusually small nuclear quadrupole coupling constants [48]. Figure 5(a) shows $R_{t0}(F)$ and $\alpha_0(F)$ from spin-free coupled-channel calculations on NaCs. Figure 5(b) shows $\delta\alpha_{jj}(F)$ from Eq. 4 for the hyperfine states with the largest and smallest values of d_j. The variation in $\alpha_{jj'}$ between spin states is only about 0.1% at most fields, and only about 3 a_0 around the zero in α.

III. MANY-BODY PHYSICS

Molecular systems with an SU(N) symmetry offer vast new possibilities for quantum simulation and many-body physics. The large spin degeneracy and the high symmetry enhance quantum fluctuations, stabilize exotic states of matter such as chiral spin liquids [13, 14], and produce interesting dynamics, such as controllable prethermalization [49]. Experiments will fall into two categories: experiments in continuous space with just a trap, and optical lattice experiments.

In continuum experiments, the use of molecules will enrich the SU(N) phenomena studied with alkaline-earth atoms and also allow exploration of totally new areas. Ref. [50] has demonstrated quantum gas microscopy, which remains in development for fermionic alkaline-earth atoms. The large number of hyperfine states will allow exploration of repulsive SU(N) models with much larger N than for alkaline-earth atoms; this will enhance quantum fluctuations and topological order [13, 14]. The larger N may also allow even lower temperatures than in alkaline-earth atoms, which already reach record-low temperatures for fermions [12].

Attractive and bosonic systems are also rich areas. Attractive gases, both with and without an optical lattice, may allow experiments to explore the formation of energetically favorable clusters and their ordering, with connections to both condensed [36–41] and high-density nuclear matter [42]. Bosonic SU(N) systems have been considered, for example as integrable systems [43], non-Abelian ferromagnets [45] and holographic duals [44].

To explore these areas efficiently and connect experiments to models studied in many-body physics, it is necessary to reduce the coupled-channel results to an effective interaction. This is analogous to replacing the complicated interatomic potential for atoms with a delta-function. Due to the range of thousands of bohr and $1/R^4$ tail, a contact potential is probably adequate only for very dilute gases. The strength of the delta-function interaction can be determined from the scattering length

in the coupled-channel calculations. Higher densities will probably require more accurate effective potentials based on the complete adiabats.

Optical lattice experiments with molecules provide another wide-ranging arena for SU(N) many-body physics. In a sufficiently deep lattice, with temperatures and interactions small compared to the band gap, the system is described by an SU(N) Hubbard Hamiltonian,

$$\hat{H} = -t \sum_{\langle i,j\rangle,\sigma} \left(\hat{c}^\dagger_{i\sigma}\hat{c}_{j\sigma} + \text{h.c.}\right) + \frac{U}{2}\sum_{i,\sigma,\tau} \hat{n}_{i\sigma}\hat{n}_{i\tau} + \sum_{ij;\sigma\tau} \frac{V_{ij}}{2} n_{i\sigma}n_{j\tau} + \sum_{i\sigma}(\epsilon_\sigma - \mu_\sigma)\hat{n}_{i\sigma}, \quad (6)$$

where $c_{i\sigma}$ and $c^\dagger_{i\sigma}$ are annihilation and creation operators at site i for hyperfine state σ, and $n_{i\sigma} = c^\dagger_{i\sigma}c_{i\sigma}$, $V_{ij} = C_3(1-3\cos^2(\Theta_{ij}))/|\vec{r}_i - \vec{r}_j|^3$ with Θ_{ij} the angle between the intermolecular separation and the electric field is the dipole interaction between molecules i and j, and ϵ_σ and μ_σ are the number operator, single-molecule energy and chemical potential for component σ. The tunneling energy t is

$$t = -\int d^3r\, w^*(\boldsymbol{r}) \left(-\frac{\hbar^2}{2m} + V(\boldsymbol{r})\right) w(\boldsymbol{r}+\boldsymbol{d}), \quad (7)$$

where $\boldsymbol{d}$ is a nearest-neighbor lattice vector, m is the molecular mass, $V(\boldsymbol{r})$ is the lattice potential of a molecule at center of mass position $\vec{r}$, and $w(\boldsymbol{r})$ is the lowest-band Wannier function obtained from the single-particle band structure. When the spread of the Wannier functions is much larger than the interaction range,

$$U = \frac{4\pi\hbar^2 a}{m}\int d^3r\, |w(\boldsymbol{r})|^4, \quad (8)$$

where a is the scattering length. Due to the large spatial extent of the interaction potential, Eq. 8 may provide only a rough estimate of U. Quantitative calculations of U can be performed by solving the two-body problem numerically. This is a challenging calculation, but is tractable when the lattice is deep enough. Although the single-molecule energies in the last term of Eq. (7) apparently break SU(N) symmetry, they are irrelevant because $\hat{N}_\sigma = \sum_i \hat{n}_{i\sigma}$, is conserved.

IV. OUTLOOK

Realization of SU(N) symmetry in ultracold molecules will unlock a broad range of new physics, with strong connections to condensed matter and other areas of many-body physics.

A first step will be to confirm and quantify the degree of symmetry experimentally. Initial characterizations may be performed by measuring the kinetics of evaporation or cross-dimensional thermalization, already measured for one spin component of ^{40}KRb [29]. For a system with SU(N) symmetry, these are independent of hyperfine state. Spectroscopy can provide more accurate measurements, analogous to those for SU(N) symmetry with alkaline-earth atoms [51]. Two-photon microwave or Raman spectroscopy can measure the difference in interaction energy when the spin state is changed. A useful limit is a deep lattice where tunneling is negligible, so photons will drive one-molecule hyperfine transitions on doubly-occupied sites. Amplitude-modulation spectroscopy has also been used to measure interactions of atoms in lattices to high precision [52]. With the SU(N) symmetry confirmed, experiments can begin probing the many-body phases of matter and dynamics offered.

This work also opens areas of theoretical research in both molecular collisions and many-body physics. Although the treatment of the alkali dimers in Sec. II B is sufficient to estimate the degree of SU(N) symmetry, full coupled-channel calculations are needed for quantitative results. This challenges current methods due to the large number of nuclear states. Although we have focused here on shielding with static electric fields, we expect that microwave shielding will provide interactions with a comparable degree of SU(N) symmetry. Coupled-channel calculations are needed to verify this.

The new many-body physics offered by shielded ultracold molecules includes gases, Hubbard models, and Heisenberg models with large N. Such systems can have positive or negative scattering lengths, bosonic or fermionic or constitutents, and dipolar interactions. These offer fertile ground to study new phases and dynamics of quantum matter.

RIGHTS RETENTION STATEMENT

DATA AVAILABILITY STATEMENT

Data supporting this study are openly available from Durham University [53].

ACKNOWLEDGMENTS

K.R.A.H. acknowledges support from the National Science Foundation (PHY-1848304), the Robert A. Welch Foundation (C-1872), and the W. M. Keck Foundation (Grant No. 995764). K.R.A.H. benefited from discussions at the the Aspen Center for Physics, which is supported in part by the National Science Foundation (PHY-1066293). B.M. and J.M.H. are grateful to Matthew Frye and Ruth Le Sueur for valuable discussions and acknowledge support from the U.K. Engineering and

Physical Sciences Research Council (EPSRC) Grant Nos. EP/W00299X/1, and EP/V011677/1.

METHODS

A. Hamiltonian for the spin-free case

The Hamiltonian of spin-free CaF in an electric field is

$$\hat{h} = b\hat{\boldsymbol{n}}^2 - \boldsymbol{\mu}\cdot\boldsymbol{F}. \tag{9}$$

The molecule is treated as a rigid rotor with rotational constant b in an electric field $\boldsymbol{F}$ along the z axis; $\hat{\boldsymbol{n}}$ is the operator for molecular rotation. For ^{40}Ca^{19}F, $b/h \approx 10.267\,\mathrm{GHz}$ and $|\boldsymbol{\mu}| = 3.07\,\mathrm{D}$. The corresponding Hamiltonian for a pair of molecules is

$$\hat{h}_1 + \hat{h}_2 + \frac{\hat{\boldsymbol{L}}^2}{2\mu_{\mathrm{red}}} + \hat{H}_{\mathrm{dd}} - C_6^{\mathrm{elec}}/R^6, \tag{10}$$

where $\hat{\boldsymbol{L}}$ is the operator for relative rotation of the pair and μ_{red} is the reduced mass. C_6^{elec} accounts for the electronic dispersion interaction between the molecules [24, 54], but has only small effects on the results.

B. Basis sets used in coupled-channel calculations

The methodology used for the coupled-channel calculations on CaF is as described in Ref. [24], except that the present calculations use different basis sets.

As in Ref. [24], we use basis sets that are constructed from symmetrized products of field-dressed rotor functions $|\tilde{n}, m_n\rangle$ and spin functions $|g, m_g\rangle$, together with functions for the partial-wave quantum number L and its projection M_L. We include rotor functions with $\tilde{n}$ up to 5. For CaF, there are four spin functions for each monomer rotor state. However, the resulting number of pair basis functions, N_{pair}, is too large ($\sim$10000 for each L, M_L) to be used directly in coupled-channel calculations. We therefore include only a relatively small number of "class 1" pair functions explicitly in the basis set, with the remaining "class 2" functions taken into account through Van Vleck transformations as described in ref. [24].

It is the number of class 1 functions that determines the overall computational cost. To achieve a manageable basis-set size, we include only energetically nearby rotor pairs in class 1 and move the remainder to class 2. In the present work, we include 14 rotor pairs in class 1: $(\tilde{n}, m_n)$ = (0,0)+(1,0), (1,−1)+(1,−1), (1,1)+(1,−1), (1,1)+(1,1), (1,0)+(1,−1), (1,0)+(1,1), (1,0)+(1,0), (0,0)+(2,−1), (0,0)+(2,1), (0,0)+(2,0), (1,−1)+(2,−1), (1,−1)+(2,1), (1,1)+(2,−1) and (1,1)+(2,1). Inclusion of all spin functions for each of these rotor pairs gives a total number of symmetrized pair states $N_{\mathrm{pair}} = 206$. We refer to basis sets based on this as spin-N206.

The spin-dependence of scattering lengths, characterized by $\delta\alpha_{jj'}$, converges very fast with respect to the rotor basis, and is much better than 1% for spin-N206. The convergence of loss rates is slower, and varies with field because colliding pairs are more likely to reach short range when shielding is poor. Nevertheless, at 23 kV/cm, spin-N206 gives convergence of loss rates to within 1%.

The basis set of partial waves is also important. For each pair function (rotor plus spin), we include partial waves L up to 6 and refer to the resulting basis sets as spin-N206-L6. For each spin combination, calculations are performed for only a single value of $M_{\mathrm{tot}} = m_{n,1} + m_{n,2} + m_{g,1} + m_{g,2} + M_L$, such that the s-wave channel for the initial state is included in the basis set. The total number of coupled channels in class 1 varies from 556 to 652. Based on comparisons between spin-N206-L6 and spin-N206-L4, we estimate that spin-N206-L6 gives $\delta\alpha_{jj'}$ converged to better than 1% and loss rates converged within 10%.

C. Hamiltonian for fine and hyperfine structure

For a single CaF molecule, the Hamiltonian for fine and hyperfine structure is

$$\hat{h}_{\mathrm{fhf}} = \gamma\hat{\boldsymbol{s}}\cdot\hat{\boldsymbol{n}} + \zeta_{\mathrm{F}}\hat{\boldsymbol{i}}\cdot\hat{\boldsymbol{s}} + t\sqrt{6}T^2(C)\cdot T^2(\hat{\boldsymbol{i}}, \hat{\boldsymbol{s}}) + c_{\mathrm{F}}\hat{\boldsymbol{i}}\cdot\hat{\boldsymbol{n}}. \tag{11}$$

Here the first term represents the electron spin-rotation interaction, while the second and third terms account for the isotropic and anisotropic interactions between electron and nuclear spins. $T^2(\hat{\boldsymbol{i}}, \hat{\boldsymbol{s}})$ denotes the rank-2 spherical tensor formed from $\hat{\boldsymbol{i}}$ and $\hat{\boldsymbol{s}}$, and $T^2(C)$ is a spherical tensor whose components are the Racah-normalized spherical harmonics $C_q^2(\theta, \phi)$. The last term represents the nuclear spin-rotation interaction, which is typically three orders of magnitude smaller than the others. The values of the constants b, γ, ζ_{F}, t and c_{F} for CaF are the same as in Ref. [24].

D. Effective-potential model of spin dependence

In a semiclassical approximation [55], the real part α of the s-wave scattering length for a potential with long-range part proportional to R^{-4} may be written in terms of a phase integral Φ,

$$\alpha = R_{\mathrm{t}} - \sqrt{8/15}D\tan\left(\Phi - \frac{\pi}{4}\right). \tag{12}$$

Here R_{t} is the inner turning point at zero collision energy, with $U(R_{\mathrm{t}}) = U(\infty) = 0$, D is the dipole length, and

$$\Phi = \int_{R_{\mathrm{t}}}^{\infty} k(R)\, dR, \tag{13}$$

where $k(R) = (2\mu_{\mathrm{red}}|U(R)|/\hbar^2)^{1/2}$. The first term in Eq. 12, R_{t}, is omitted in Ref. [55], but can be a substantial

fraction of D for shielded collisions; for CaF at 23 kV/cm, with $D \approx 1290\ a_0$, R_t contributes about 380 a_0 to α.

If we take the spin-free adiabat $U_0(R)$ as a reference, with phase $k_0(R)$ and phase integral Φ_0, the integral $\Phi_{jj'}$ for a slightly shifted potential $U_{jj'}(R)$ for the interaction between species in spin states j and j' is

$$\begin{aligned}\Phi_{jj'} &= \int_{R_{\mathrm{t}jj'}}^{\infty} k_{jj'}(R)\, dR \\ &\approx \int_{R_{\mathrm{t}0}}^{\infty} k_0(R)\left[1 + \tfrac{1}{2}\Delta U_{jj'}(R)\right] dR, \end{aligned} \tag{14}$$

where $\Delta U_{jj'}(R)$ is the difference between adiabats defined by Eq. 2 of the main text.

As shown in Extended Data Figure 1, $\Phi_{jj'}$ scales approximately with $D_{jj'}^2$ and R_t scales approximately with $D_{jj'}^{-1}$. These dependences apply to varying isotopic combination at constant field, but *not* to varying field, which also changes the separation of the field-dressed states.

Differentiating Eq. 12 with these dependences on D gives

$$\begin{aligned}\frac{d\alpha}{dD} \approx& -R_\mathrm{t}/D - \sqrt{8/15}\tan\left(\Phi - \frac{\pi}{4}\right) \\ &- 2\Phi\sqrt{8/15}\sec^2\left(\Phi - \frac{\pi}{4}\right) \\ \approx& (\alpha - 2R_\mathrm{t})/D - 2\Phi\sqrt{8/15}\sec^2\left(\Phi - \frac{\pi}{4}\right). \end{aligned} \tag{15}$$

The last term is large near any poles in α; it has minima near $\Phi/\pi = \text{integer} + 1/4$, which is close to the zeroes in α, but is nevertheless usually the largest term under shielding conditions.

EXTENDED DATA

$(g, m_g) + (g', m_g')$	$D_{jj'}$	$R_{\mathrm{t}jj'}$	$\Phi_{jj'}/\pi$	$\delta\alpha_{jj'}$ (model)	$\delta\alpha_{jj'}$ (c.c.)
(0,0)+(0,0)	1292	381.7	0.6628	2.22	4.28
(0,0)+(1,0)	1293	381.4	0.6638	−46.5	−41.7
(0,0)+(1,1)	1292	381.9	0.6622	26.6	26.3
(1,0)+(1,0)	1294	381.0	0.6648	−95.3	−88.7
(1,0)+(1,1)	1293	381.6	0.6633	−22.1	−19.2
(1,1)+(1,1)	1291	382.1	0.6617	51.0	48.8
(1,1)+(1,−1)	1291	382.1	0.6617	51.0	48.8

TABLE I. **Comparing changes in scattering lengths predicted by the model with coupled-channel calculations including spin.** For CaF at 23 kV/cm, $D_0 = 1292\ a_0$, $R_{\mathrm{t}0} = 381.7\ a_0$, $\Phi_0/\pi = 0.6628$ and $\alpha_0 = -2980\ a_0$. All lengths are in units of a_0.

[1] A. V. Gorshkov, M. Hermele, V. Gurarie, C. Xu, P. S. Julienne, J. Ye, P. Zoller, E. Demler, M. D. Lukin, and A. Rey, Two-orbital SU(N) magnetism with ultracold alkaline-earth atoms, Nature Physics **6**, 289 (2010).

[2] M. A. Cazalilla, A. Ho, and M. Ueda, Ultracold gases of ytterbium: ferromagnetism and Mott states in an SU(6) Fermi system, New Journal of Physics **11**, 103033 (2009).

[3] C. Wu, J.-P. Hu, and S.-C. Zhang, Exact SO(5) symmetry in the spin-3/2 fermionic system, Physical Review Letters **91**, 186402 (2003).

[4] M. A. Cazalilla and A. M. Rey, Ultracold Fermi gases with emergent SU(N) symmetry, Reports on Progress in Physics **77**, 124401 (2014).

[5] B. Song, Y. Yan, C. He, Z. Ren, Q. Zhou, and G.-B. Jo, Evidence for bosonization in a three-dimensional gas of SU(N) fermions, Physical Review X **10**, 041053 (2020).

[6] C. He, Z. Ren, B. Song, E. Zhao, J. Lee, Y.-C. Zhang, S. Zhang, and G.-B. Jo, Collective excitations in two-dimensional SU(N) Fermi gases with tunable spin, Physical Review Research **2**, 012028 (2020).

[7] G. Pagano, M. Mancini, G. Cappellini, P. Lombardi, F. Schäfer, H. Hu, X.-J. Liu, J. Catani, C. Sias, M. Inguscio, *et al.*, A one-dimensional liquid of fermions with tunable spin, Nature Physics **10**, 198 (2014).

[8] D. Tusi, L. Franchi, L. Livi, K. Baumann, D. Benedicto Orenes, L. Del Re, R. Barfknecht, T.-W. Zhou, M. Inguscio, G. Cappellini, *et al.*, Flavour-selective localization in interacting lattice fermions, Nature Physics **18**, 1201 (2022).

[9] S. Taie, R. Yamazaki, S. Sugawa, and Y. Takahashi, An SU(6) Mott insulator of an atomic Fermi gas realized by large-spin Pomeranchuk cooling, Nature Physics **8**, 825 (2012).

[10] C. Hofrichter, L. Riegger, F. Scazza, M. Höfer, D. R. Fernandes, I. Bloch, and S. Fölling, Direct probing of the Mott crossover in the SU(N) Fermi-Hubbard model, Physical Review X **6**, 021030 (2016).

[11] G. Pasqualetti, O. Bettermann, N. Darkwah Oppong, E. Ibarra-García-Padilla, S. Dasgupta, R. T. Scalettar, K. R. A. Hazzard, I. Bloch, and S. Fölling, Equation of state and thermometry of the 2d SU(N) Fermi-Hubbard model, Physical Review Letters **132**, 083401 (2024).

[12] S. Taie, E. Ibarra-García-Padilla, N. Nishizawa, Y. Takasu, Y. Kuno, H.-T. Wei, R. T. Scalettar, K. R.

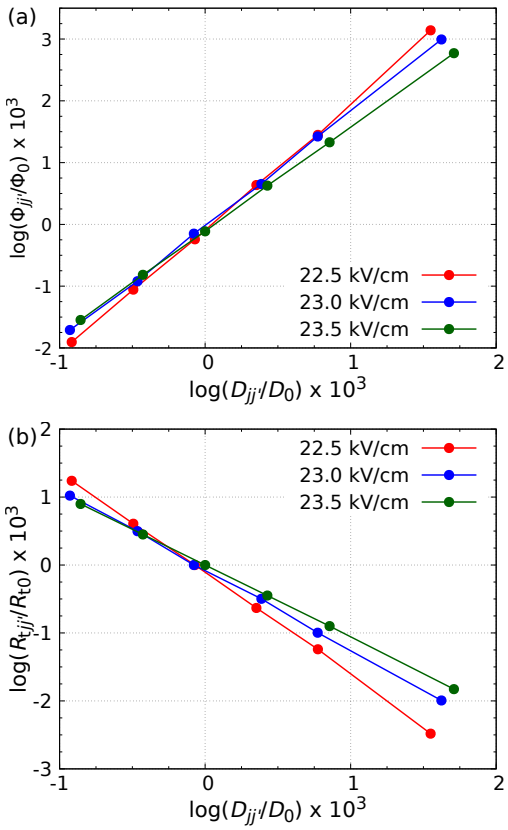

FIG. 1. **Dependence of phase integral and inner turning point for CaF on dipole length.** (a) Phase integrals $\Phi_{jj'}$ and (b) inner turning points $R_{tjj'}$ for different spin states j as a function of dipole length $D_{jj'}$, for three different electric fields in the shielding region. All quantities are expressed as ratios to their spin-free values. The slopes of the plots show that, at each field, $\Phi_{jj'}$ scales approximately as $D_{jj'}^2$ and $R_{tjj'}$ scales approximately as $D_{jj'}^{-1}$.

Hazzard, and Y. Takahashi, Observation of antiferromagnetic correlations in an ultracold SU(N) Hubbard model, Nature Physics **18**, 1356 (2022).

[13] M. Hermele, V. Gurarie, and A. M. Rey, Mott insulators of ultracold fermionic alkaline earth atoms: Underconstrained magnetism and chiral spin liquid, Physical Review Letters **103**, 135301 (2009).

[14] G. V. Chen and C. Wu, Multiflavor Mott insulators in quantum materials and ultracold atoms, npj Quantum Materials **9**, 1 (2024).

[15] K. Heyde, *Basic ideas and concepts in nuclear physics: an introductory approach* (CRC Press, 2020).

[16] T. Langen, G. Valtolina, D. Wang, and J. Ye, Quantum state manipulation and science of ultracold molecules, arXiv preprint arXiv:2305.13445 (2023).

[17] C. P. Koch, M. Lemeshko, and D. Sugny, Quantum control of molecular rotation, Reviews of Modern Physics **91**, 035005 (2019).

[18] G. Quéméner and P. S. Julienne, Ultracold molecules under control!, Chemical Reviews **112**, 4949 (2012).

[19] M. L. Wall, K. R. A. Hazzard, and A. M. Rey, From atomic to mesoscale: The role of quantum coherence in systems of various complexities (World Scientific, 2015) Chap. Quantum magnetism with ultracold molecules.

[20] S. L. Cornish, M. R. Tarbutt, and K. R. A. Hazzard, Quantum computation and quantum simulation with ultracold molecules, arXiv preprint arXiv:2401.05086.

[21] A. V. Avdeenkov, M. Kajita, and J. L. Bohn, Suppression of inelastic collisions of polar $^1\Sigma$ state molecules in an electrostatic field, Physical Review A **73**, 022707 (2006).

[22] G. Wang and G. Quéméner, Tuning ultracold collisions of excited rotational dipolar molecules, New Journal of Physics **17**, 035015 (2015).

[23] M. L. González-Martínez, J. L. Bohn, and G. Quéméner, Adimensional theory of shielding in ultracold collisions of dipolar rotors, Physical Review A **96**, 032718 (2017).

[24] B. Mukherjee, M. D. Frye, C. R. Le Sueur, M. R. Tarbutt, and J. M. Hutson, Shielding collisions of ultracold CaF molecules with static electric fields, Physical Review Research **5**, 033097 (2023).

[25] B. Mukherjee and J. M. Hutson, Controlling collisional loss and scattering lengths of ultracold dipolar molecules with static electric fields, Physical Review Research **6**, 013145 (2024).

[26] T. Karman and J. M. Hutson, Microwave shielding of ultracold polar molecules, Physical Review Letters **121**, 163401 (2018).

[27] L. Lassablière and G. Quéméner, Controlling the scattering length of ultracold dipolar molecules, Physical Review Letters **121**, 163402 (2018).

[28] K. Matsuda, L. D. Marco, J.-R. Li, W. G. Tobias, G. Valtolina, G. Quéméner, and J. Ye, Resonant collisional shielding of reactive molecules using electric fields, Science **370**, 1324 (2020).

[29] G. Valtolina, K. Matsuda, W. G. Tobias, J.-R. Li, L. De Marco, and J. Ye, Dipolar evaporation of reactive molecules to below the Fermi temperature, Nature **588**, 239 (2020).

[30] J.-R. Li, W. G. Tobias, K. Matsuda, C. Miller, G. Valtolina, L. D. Marco, R. R. W. Wang, L. Lassablière, G. Quéméner, J. L. Bohn, and J. Ye, Tuning of dipolar interactions and evaporative cooling in a three-dimensional molecular quantum gas, Nature Physics **17**, 1144 (2021).

[31] L. Anderegg, S. Burchesky, Y. Bao, S. S. Yu, T. Karman, E. Chae, K.-K. Ni, W. Ketterle, and J. M. Doyle, Observation of microwave shielding of ultracold molecules, Science **373**, 779 (2021).

[32] A. Schindewolf, R. Bause, X.-Y. Chen, M. Duda, T. Karman, I. Bloch, and X.-Y. Luo, Evaporation of microwave-shielded polar molecules to quantum degeneracy, Nature **607**, 677 (2022).

[33] N. Bigagli, C. Warner, W. Yuan, S. Zhang, I. Stevenson, T. Karman, and S. Will, Collisionally stable gas of bosonic dipolar ground state molecules, Nature Physics **19**, 1579 (2023).

[34] J. Lin, G. Chen, M. Jin, Z. Shi, F. Deng, W. Zhang, G. Quéméner, T. Shi, S. Yi, and D. Wang, Microwave shielding of bosonic NaRb molecules, Physical Review X **13**, 031032 (2023).

[35] N. Bigagli, W. Yuan, S. Zhang, B. Bulatovic, T. Karman, I. Stevenson, and S. Will, Observation of Bose-Einstein condensation of dipolar molecules, arXiv preprint arXiv:2312.10965.

[36] J. Pohlmann, A. Privitera, I. Titvinidze, and W. Hofstetter, Trion and dimer formation in three-color fermions, Physical Review A **87**, 023617 (2013).

[37] A. Rapp, G. Zaránd, C. Honerkamp, and W. Hofstetter, Color superfluidity and "baryon" formation in ultracold fermions, Physical Review Letters **98**, 160405 (2007).

[38] K. Inaba and S.-I. Suga, Finite-temperature properties of attractive three-component fermionic atoms in optical lattices, Physical Review A **80**, 041602 (2009).

[39] I. Titvinidze, A. Privitera, S.-Y. Chang, S. Diehl, M. Baranov, A. Daley, and W. Hofstetter, Magnetism and domain formation in SU(3)-symmetric multi-species Fermi mixtures, New Journal of Physics **13**, 035013 (2011).

[40] A. Koga and H. Yanatori, Spontaneously symmetry-breaking states in the attractive SU(N) Hubbard model, Journal of the Physical Society of Japan **86**, 034702 (2017).

[41] H. Xu, X. Li, Z. Zhou, X. Wang, L. Wang, C. Wu, and Y. Wang, Trion states and quantum criticality of attractive SU(3) Dirac fermions, Physical Review Research **5**, 023180 (2023).

[42] Y. Aoki, G. Endrődi, Z. Fodor, S. D. Katz, and K. K. Szabó, The order of the quantum chromodynamics transition predicted by the standard model of particle physics, Nature **443**, 675 (2006).

[43] Z. Maassarani, Exact integrability of the $su(n)$ Hubbard model, Modern physics letters B **12**, 51 (1998).

[44] M. Fujita, R. Meyer, S. Pujari, and M. Tezuka, Effective hopping in holographic Bose and Fermi-Hubbard models, Journal of High Energy Physics **2019**, 1 (2019).

[45] A. P. Polychronakos and K. Sfetsos, Ferromagnetic phase transitions in SU(N), Nuclear Physics B **996**, 116353 (2023).

[46] S. Yi and L. You, Trapped atomic condensates with anisotropic interactions, Physical Review A **61**, 041604(R) (2000).

[47] J. Aldegunde, B. A. Rivington, P. S. Żuchowski, and J. M. Hutson, Hyperfine energy levels of alkali metal dimers: ground-state polar molecules in electric and magnetic fields, Physical Review A **78**, 033434 (2008).

[48] J. Aldegunde and J. M. Hutson, Hyperfine structure of alkali-metal diatomic molecules, Physical Review A **96**, 042506 (2017).

[49] C.-H. Huang, Y. Takasu, Y. Takahashi, and M. A. Cazalilla, Suppression and control of prethermalization in multicomponent Fermi gases following a quantum quench, Physical Review A **101**, 053620 (2020).

[50] L. Christakis, J. S. Rosenberg, R. Raj, S. Chi, A. Morningstar, D. A. Huse, Z. Z. Yan, and W. S. Bakr, Probing site-resolved correlations in a spin system of ultracold molecules, Nature **614**, 64 (2023).

[51] X. Zhang, M. Bishof, S. L. Bromley, C. V. Kraus, M. S. Safronova, P. Zoller, A. M. Rey, and J. Ye, Spectroscopic observation of SU(N)-symmetric interactions in Sr orbital magnetism, Science **345**, 1467 (2014).

[52] M. J. Mark, E. Haller, K. Lauber, J. G. Danzl, A. J. Daley, and H.-C. Nägerl, Precision measurements on a tunable Mott insulator of ultracold atoms, Physical Review Letters **107**, 175301 (2011).

[53] B. Mukherjee, J. M. Hutson, and K. R. A. Hazzard, `https://collections.durham.ac.uk/files/r1hq37vn60c`, supporting data for "SU(N) magnetism with ultracold molecules".

[54] M. Lepers, R. Vexiau, M. Aymar, N. Bouloufa-Maafa, and O. Dulieu, Long-range interactions between polar alkali-metal diatoms in external electric fields, Physical Review A **88**, 032709 (2013).

[55] G. F. Gribakin and V. V. Flambaum, Calculation of the scattering length in atomic collisions using the semiclassical approximation, Physical Review A **48**, 546 (1993).